Journal of Solid State Chemistry 184 (2011) 1931–1938

Contents lists available at ScienceDirect

Journal of Solid State Chemistry

journal homepage: www.elsevier.com/locate/jssc

Photoluminescence and energy transfer in Tb^{3+}/Mn^{2+} co-doped $ZnAl_2O_4$ glass ceramics

Gandham Lakshminarayana, Lothar Wondraczek*

Department of Materials Science, University of Erlangen-Nuremberg, Erlangen 91058, Germany

ARTICLE INFO

Article history:
Received 24 January 2011
Received in revised form
11 April 2011
Accepted 29 May 2011
Available online 6 June 2011

Keywords:
Phosphor
Glass ceramic
Rare earth
Transition metal
Energy transfer
Lighting

ABSTRACT

We report on Tb^{3+} as efficient sensitizer for red photoemission from Mn^{2+}-centers in $ZnO–B_2O_3–Al_2O_3–Si_2O–Na_2O–SrO$ glasses and corresponding gahnite glass ceramics. In comparison to singly or co-doped glasses, the glass ceramics exhibit significantly increased emission intensity. Structural considerations, ESR, and dynamic luminescence spectroscopy indicate partial incorporation of Mn^{2+} as well as Tb^{3+} into the crystalline phase, the former on octahedral Zn^{2+}-sites. Interionic distance and charge transfer probability between both species depend on crystallization conditions. This enables control of the energy transfer process and, hence, tunability of the color of photoemission by simultaneous emission from Tb^{3+} and Mn^{2+} centers. Concentration quenching in Mn^{2+}-singly doped materials was found at a critical dopant concentration of about 1.0 mol%. The energy transfer process was studied in detail by dynamic as well as static luminescence spectroscopy. Spectroscopic results suggest the application of the studied materials as single or dual-mode emitting phosphor for luminescent lighting.

1. Introduction

Zinc aluminate ($ZnAl_2O_4$) is a wide-band gap semiconductor (E_g=3.8 eV), which occurs naturally as the mineral gahnite and is a member of the spinel family. Spinels represent an important class of chemically and thermally stable crystalline materials. The interaction between ZnO and Al_2O_3 to form $ZnAl_2O_4$ spinel (cubic, space group $Fd3m$, a=8.088 Å) follows diffusion of Zn and O and an effective unilateral transfer of ZnO [1] as shown in Fig. 1. Of the contributing cations, Zn^{2+} is tetrahedrally coordinated and Al^{3+} occupies octahedral sites [2]. Occupation (or substitution) of these two sites is decided by various factors, such as ionic size, cationic charge, electron distribution and electronic state [3], and gahnite and other spinels provide a suitable host lattice for various dopant species, e.g., luminescence properties of rare-earth doped zinc spinels have been reported recently [4–6]. By precipitating gahnite crystals from a transition metal (TM) or rare earth (RE) doped glass melt and partitioning the dopant species into the crystal phase, their optical activity can typically be enhanced significantly [7–18].

The ground state of the Mn^{2+} ion is $^6A_{1g}$ (spherically non-degenerated, octahedral symmetry). As all of the excited states are quartets or doublets, the optical absorption spectra of Mn^{2+} ions exhibit only spin forbidden transitions [19]. Excitation bands lie in the UV–Vis spectral region, and photoluminescence typically results from the $^4T_{1g}(G)\rightarrow{}^6A_{1g}(S)$ transition [20]. This transition becomes partially allowed as a result of spin–orbit interactions. Typically, d–d transitions are strongly dependent on the field strength of the surrounding ligands because the d-shell is only weakly shielded from its environment. In Mn^{2+}, its spectral position can vary from green to deep red color, depending on coordination and ligand field strength. Usually, tetrahedral coordination ($^{IV}Mn^{2+}$, weak crystal field) results in green emission whereas octahedral coordination ($^{VI}Mn^{2+}$, stronger crystal field) results in orange to red emission [19]. Over decades, this property has made Mn^{2+}-doped materials one of the most important types of phosphors in lighting and display applications [21]. On the other hand, Tb^{3+} exhibits a relatively simple energy level structure with the ground state $^7F_6$, and several other low-lying excited states (i.e., $^5D_{4,\ 3,\ 2,\ 1}$, $^5L_{10}$, $^5G_6$, $^5L_9$, etc.). Typically, Tb^{3+}-doped materials show intense photoluminescence in the green spectral region [22]. In a co-doped material, energy transfer from one ion (sensitizer) to another ion (activator) may occur, in principle, in whole or partly by non-radiative and/or radiative processes [23–25]. Such energy transfer processes have recently received significant attention, involving ion pairs such as Eu^{2+}/Mn^{2+} [26,27], Sm^{3+}/Tb^{3+} [28], Ce^{3+}/Tb^{3+} [29], Tb^{3+}/Eu^{3+} [30], and Ce^{3+}/Eu^{2+} [31,32]. Due to the forbidden $^4T_1\rightarrow{}^6A_1$ transition of Mn^{2+}, the fluorescence intensity of Mn^{2+} singly doped materials is low under UV excitation. An efficient sensitizer would significantly enhance red photoemission from Mn^{2+} also under UV

* Corresponding author. Fax: +49 9131 28311.
E-mail address: lothar.wondraczek@ww.uni-erlangen.de (L. Wondraczek).

0022-4596/$ - see front matter © 2011 Elsevier Inc. All rights reserved.
doi:10.1016/j.jssc.2011.05.059

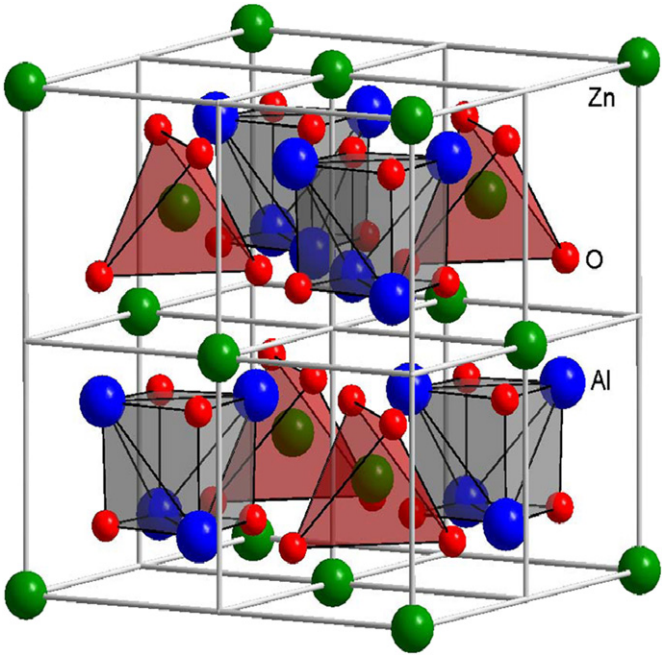

Fig. 1. Crystal structure of $ZnAl_2O_4$.

excitation. Regarding electronic structure, Tb^{3+} represents a suitable sensitizer for photoemission from Mn^{2+}, and has therefore been considered for this purpose on several occasions [25]. The present report therefore focuses on the detailed investigation of luminescence properties and color tunability of Tb^{3+}/Mn^{2+}-codoped zinc–boroaluminosilicate glasses and corresponding glass ceramics.

2. Experimental

Glasses of nominal composition (mol%) $30B_2O_3$–$10SiO_2$–$10Al_2O_3$–$30ZnO$–$10Na_2O$–$(10-x-y)SrO$–$xMnO$–yTb_2O_3 (ZABS) were prepared from reagent grade B_2O_3, ZnO, SiO_2, Al_2O_3, Na_2CO_3, $SrCO_3$, $MnCO_3$, and Tb_4O_7 ($x=0$, 0.05, 0.1, 0.25, 0.5, and 1.0; $y=0$ and 0.025). Sample nomenclature is given in Table 1. Powder batches of 20 g were mixed thoroughly in an agate mortar before melting in alumina crucibles at 1460 °C for 1 h in air and quenched on a cold steel plate by immediately pressing with another steel plate. Obtained glass disks were 2–3 cm in diameter and had a thickness of about 0.2 cm. To release internal stresses, they were annealed at 525 °C for 3 h. Glass ceramics were prepared by heat-treatment of polished (SiC/water) specimens on alumina substrates at temperatures of 750 and 800 °C, each for 3 h in air. Subsequently, samples were cooled to room temperature at ~2 K/min. The density of the precursor glass was determined by the Archimedes method using distilled water as immersion liquid. An Abbe refractometer was used to measure the refractive index n_D (589.3 nm). Structural analysis was carried out by X-ray diffractometry (XRD, Siemens Kristalloflex D500, Bragg-Brentano, 30 kV/30 mA, Cu$K\alpha$), and infrared (IR) absorption spectroscopy (FTIR, Pekin-Elmer 1600) in the wave number range 400–4000 cm^{-1} with a resolution of 4 cm^{-1}. Electron spin resonance spectra (ESR) were recorded on an X-band microwave spectrometer at a frequency of 9.7 GHz (Bruker ESR 300E). Differential scanning calorimetry (DSC, Netzsch DSC 404 F1) was carried out to obtain glass transition (T_g) and crystallization onset temperatures (T_c). Absorption spectra were measured on a double-beam, double-monochromator, ratio recording UV–vis/NIR spectrophotometer (Perkin Elmer Inc., Massachusetts). Photoluminescence (excitation and emission spectra) and fluorescence decay kinetics were studied with a spectrofluorometer equipped with double monochromators (Czerny–Turner) in excitation and emission (Fluorolog-3, Horiba Jobin Yvon, spectral resolution of ~0.1 nm), using a 400 W Xe-lamp for static and a 75 W Xe-flashlamp, respectively, as excitation sources. All the measurements were performed at room temperature.

Table 1
Nominal composition of examined glasses/glass ceramics.

$0B_2O_3$–$10SiO_2$–$10Al_2O_3$–$30ZnO$–$10Na_2O$–$(10-x-y)SrO$–$xMnO$–yTb_2O_3(mol%)		
Sample code	x	y
a	0.05	
b	0.1	
c	0.25	
d	0.5	
e	1.0	
f	0.025	
g	0.05	0.025
h	0.1	0.025
i	0.25	0.025
j	0.5	0.025
k	1.0	0.025

Table 2
Basic physical properties of 0.05 mol% Mn^{2+} doped glass.

Parameters	Data
Density (g/cm^3)	3.142
Specimen thickness	0.3
Refractive index, n_D (589.3 nm)	1.455
Molar volume, V_m (cm^3/mol)	24.867
Molar refractivity, R_m (cm^{-3})	6.747
Molar polarizability, α_m (Å^3)(10^{-24})	2.676
Reflection losses, R (%)	3.435
Manganese ion concentration, N (10^{22} ions/cm^3)	2.422
Polaron radius, r_p (Å)	1.393
Interionic distance, r_i (Å)	3.457
Glass transition temperature (T_g) (°C)	535
Crystallization onset temperature (T_x) (°C)	625
Maximum crystallization temperature (T_c) (°C)	820

3. Results and discussion

3.1. General

Basic physical properties of the as-made ZABS glass are listed in Table 2. ESR analyses of specimens with differing manganese dopant concentration reveal a pronounced hyperfine sextet structure, located at field strength of about 3400 G ($g \approx 2$, Fig. 2). This is a typical indicator of the presence of paramagnetic ([Ar] $3d^5$) Mn^{2+} centers in octahedral coordination (e.g., [33]). The ground state of Mn^{2+}, ^6S, is unique among d^n configurations in which there is only one state with maximum spin multiplicity ($^6S_{5/2}$). The sextet hyperfine structure (hfs) is due to the interaction of the electron spin of Mn^{2+} with its own nuclear spin $I=5/2$ [34]. Since the total spin is 5/2, the ion exhibits zero field splitting, sensitive to the local environment. Undoped glasses or Tb^{3+}-singly doped glasses did not exhibit EPR activity in the considered range of field strengths, and also Tb^{3+}-co-doping did not have any detectable impact on the observed spectra at the employed measuring conditions. As the concentration of Mn^{2+} concentration increases up to 1.0 mol%, the intensity of the resonance signal gradually decreases due to concentration quenching by increasing interaction between neighboring Mn^{2+} centers [35]. As will be discussed later, this is confirmed by a red-shift of the related photoluminescence band.

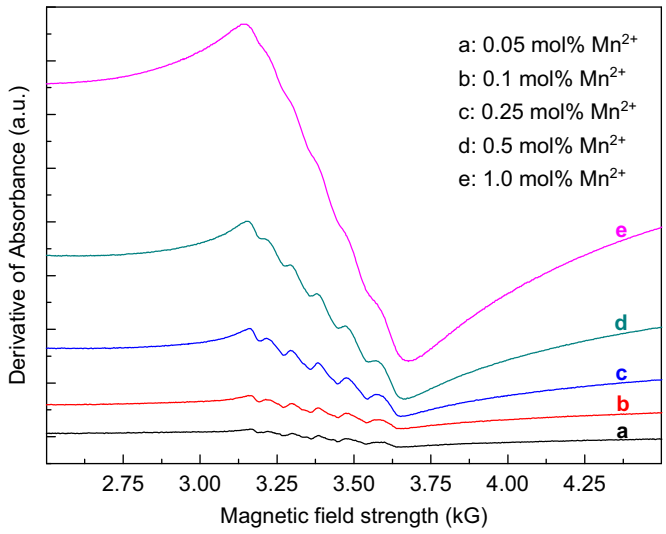

Fig. 2. ESR spectra of Mn^{2+} singly doped ZABS glasses.

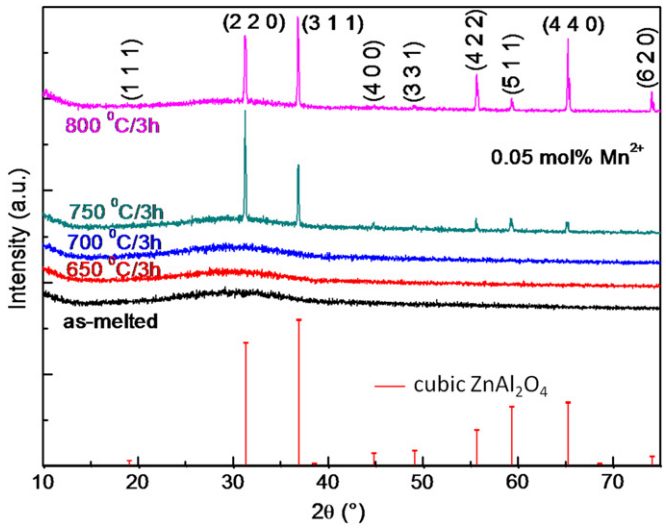

Fig. 3. XRD pattern of ZABS: 0.05 mol% Mn^{2+} for various heat treatment temperatures.

As-made glasses appeared visually transparent and colorless for a manganese concentration of less than 1 mol%. The sample with 1 mol% manganese (expressed as Mn^{2+}) exhibited a pale violet tint, originating from a broad absorption band at ~480 nm. This band can readily be attributed to the presence of traces of Mn^{3+}, caused by incomplete reduction. Colouration results from $[Ar]3d^4$, $^5E \rightarrow {}^5T_2$, which exhibits a very high absorption cross section and, hence, is visible even when only a small fraction of all Mn^{2+} species are oxidized to Mn^{3+}. Addition of larger amounts of Tb_4O_7 appeared to slightly increase the amount of Mn^{3+}, probably as a result of Tb^{4+}-reduction.

While as-made glasses are visually transparent, upon annealing and depending on heat treatment temperature and dwell time, they turn increasingly opalescent (see also [36]). This is a qualitative indicator for the precipitation of a secondary phase with a precipitate size of $> \lambda/4$ (where λ is the observation wavelength). Yellowish color in transmission indicates scattering in the blue spectral range and, hence, a crystallite size of 50–100 nm. Fig. 3 presents corresponding XRD patterns (exemplarily for glass 0.05 mol% Mn^{2+} singly doped glass) for various annealing states. While the as-made glass remains fully amorphous (no apparent diffraction peaks) for heat-treatment at up to 700 °C, heat treatment at 750–800 °C resulted in the appearance of sharp diffraction peaks. These can readily be assigned to cubic $ZnAl_2O_4$ (gahnite, JCPDS card no. 00-5-669) [37]. Noteworthy, no secondary crystalline species (such as, e.g., Zn_2SiO_4 or $Zn_3B_2O_6$) could be detected in the heat-treated samples. The average crystallite size was estimated from the FWHM of the diffraction peaks using the Scherrer equation:

$$D_{hkl} = k\lambda/[\beta(2\theta)\cos\theta],$$

where $\beta(2\theta)$ is the width of the pure diffraction profile in radians, k is the constant (0.89), λ is the wavelength of the employed X-rays (0.15418 nm), θ is the diffraction angle, and $D_{h\ k\ l}$ is the average crystallite size along the (h k l) direction [38]. The diffraction peak around 2θ–36.9 corresponding to the (3 1 1) plane was used to calculate the average crystallite sizes at various temperatures. The obtained value lies at about 50–52 nm for glass heat-treated at 750 and 800 °C. In a first consideration Mn^{2+} (ionic radius in octahedral coordination of 0.80 Å) is supposed to replace Zn^{2+} on octahedral network sites of the gahnite phase (ionic radius of 0.74 Å).

3.2. Photoluminescence of singly doped precursor glasses

In the first step, spectral luminescence properties of singly Mn^{2+} and Tb^{3+}-doped materials are considered in order to establish the basis for the interpretation of the energy transfer processes:

3.2.1. Mn^{2+}-doping

Photo-excitation and -emission schemes of Mn^{2+}-singly doped ZABS are summarized in Fig. 4.

Monitoring photoemission at 627 nm, excitation bands are found at 350–357.5, 361–374, and 414 nm (Fig. 4A). These are attributed to $^6A_1(S) \rightarrow {}^4E(D)$, $^6A_1(S) \rightarrow {}^4T_2(D)$, and $^6A_1(S) \rightarrow {}^4A_1(G)$, $^4E(G)$ in Mn^{2+}, respectively [25,27,33]. Photoemission is dominated by rather broad bands (Fig. 4B and C). When excited with UV light, aside from the dominant red emission, two minor emission bands are observed at 413 and 435 nm (Fig. 4B). These are assigned to the transitions $^4A_1(G), {}^4E(G) \rightarrow {}^6A_1(S)$, and $^4T_2(G) \rightarrow {}^6A_1(S)$, respectively. The occurrence of red photoemission is the typical result of spin forbidden $^4T_1(G) \rightarrow {}^6A_1(S)$ transition in octahedrally coordinated Mn^{2+} ions [33]. Emission intensity increases with increasing dopant concentration and reaches a maximum at 0.5 mol% of Mn^{2+}. Concentration quenching is observed when the Mn^{2+} concentration reaches 1.0 mol%. The red shift of the dominant emission peak reflects a change in ligand field strength as a result of concentration-dependent exchange interactions between neighboring Mn^{2+} ions [39–41]. Transformation of the as-melted glass into a glass ceramic results in distinct changes of the emission behavior. Firstly, for equivalent dopant concentration, the observed absolute emission intensity is several times higher. In a first consideration, this can be attributed to multiple scattering of the incoming light (e.g., [33]). Secondly, a light red-shift occurs in the static emission spectrum. Most important, however, are the changes that occur in decay behavior and emission lifetimes (here, the fluorescence lifetime is defined as the time required for the fluorescence intensity to decay down to $1/e$ of its initial value). In as-melted glasses, decay follows a single exponential equation with a lifetime of 5.60 ms, indicating that only one single type of Mn^{2+} centers is present. After crystallization, an increase occurs in emission lifetime (i.e., to 6.54 ms for 0.5 mol% Mn^{2+} after 3 h/800 °C) and decay deviates from single exponential behavior. Spectral decay analyses (Fig. 5) reveal that with increasing delay time, the emission peak shifts from 609 to 617 nm, whereby the

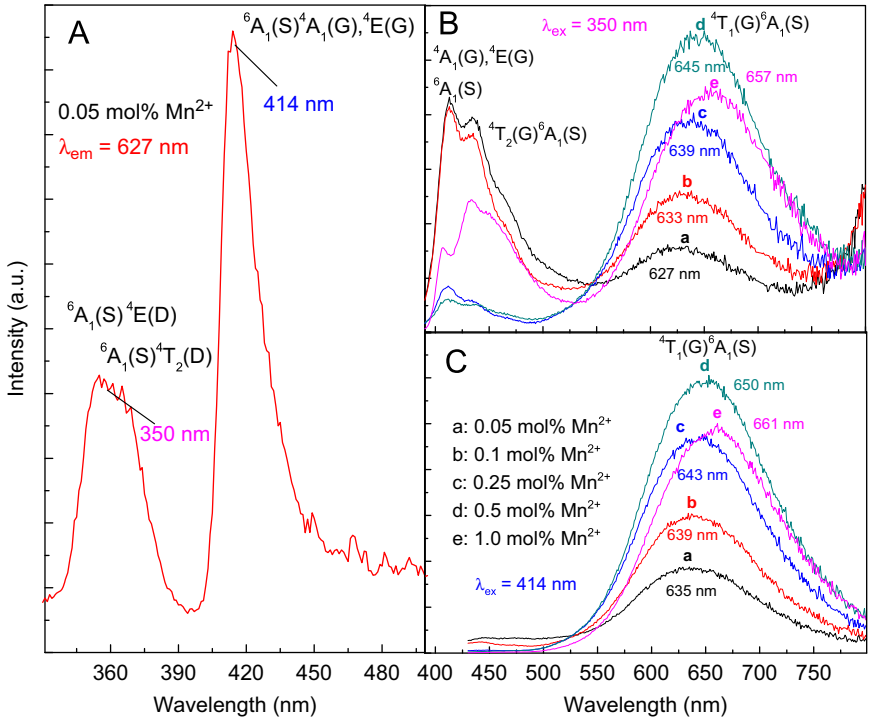

Fig. 4. Excitation spectrum of Mn^{2+} singly doped ZABS glass (A) and corresponding emission spectra for various Mn^{2+} concentrations under 350 nm (B) and 414 nm (C) excitation.

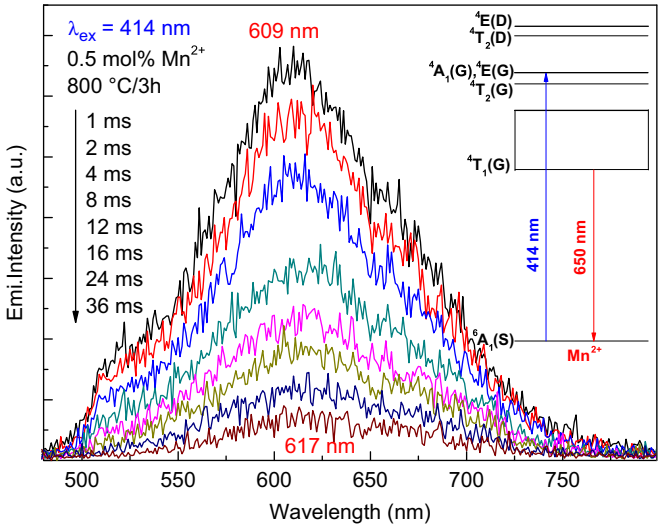

Fig. 5. Time resolved emission spectra of an Mn^{2+} singly doped ZABS glass ceramic under 414 nm excitation. Inset: Schematic of the corresponding energy levels.

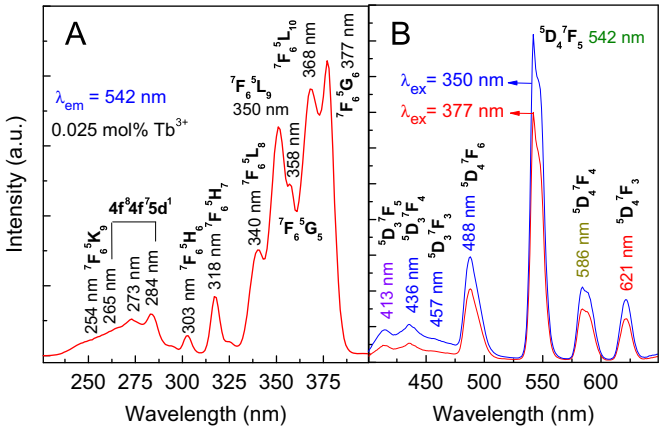

Fig. 6. Excitation spectrum of Tb^{3+} singly doped ZABS glass (A) and corresponding emission spectra for 350 and 377 nm excitation (B).

617 nm peak becomes dominant for a delay of 4 ms or longer. In particular the latter two observations may be taken as an evidence for the incorporation of Mn^{2+} ions into the nanocrystalline gahnite phase.

3.2.2. Tb^{3+} doping

Fig. 6 presents the excitation and emission spectra of Tb^{3+} singly doped ZABS. Excitation peaks associated with transitions from the $^7F_6(4f^8)$ ground state of Tb^{3+} to higher lying levels of $4f^7 5d^1$ (254–284 nm, dipolar electric parity allowed *f–d* transitions) and $4f^8$ (300–377 nm) configurations [42,43]. Maximum excitation intensity occurs at 377 nm (Fig. 6A). Emission spectra of Tb^{3+} doped ZBAS were recorded by exciting the sample at 377 nm ($^7F_6 \rightarrow {}^5G_6$) and 350 nm ($^7F_6 \rightarrow {}^5L_9$) (Fig. 6B). After excitation to any level above $^5D_3$, non-radiative decay occurs to this emitting level. In the present case, each spectrum can be divided into two parts. Blue emission between 400 and 470 nm is due to transitions from the $^5D_3$ excited state. Above 475 nm, emission peaks originate from $^5D_4$. The $^5D_3 \rightarrow {}^7F_{J(J=5,\,4,\,3)}$ emissions at 413, 436, and 457 nm and $^5D_4 \rightarrow {}^7F_{J(J=6,\,5,\,4,\,3)}$ emissions at 488, 542, 586, and 621 nm are identified from the collected emission spectra. Here, the green band of $^5D_4 \rightarrow {}^7F_5$ at 542 nm is the most intense. The energy gap below the $^5D_4$ level is ~14,600 cm^{-1}, one of the largest gaps in the energy level schemes of the RE^{3+} series. It results in intense visible emission due to low non-radiative losses. The parallel observation of emission from the $^5D_3$ level is due to slow non-radiative relaxation of $^5D_3$ to $^5D_4$. This transition is promoted by excitation of $^7F_6$ to $^7F_0$ via cross-relaxation (CR).

CR is induced by resonance of the excited states and the ground states of two Tb^{3+} ions as stated below [44–46]:

$$^5D_3 \rightarrow {}^5D_4 \Rightarrow {}^7F_6 \rightarrow {}^7F_0 \text{ and/or}$$

$$^5D_3 \rightarrow {}^7F_0 \Rightarrow {}^7F_6 \rightarrow {}^5D_4 \quad (1)$$

However, here, the probability of CR, which is inversely proportional to the sixth power of the interionic distance between dopant species, is low due to relatively low dopant concentration [47]. For a dopant concentration of 0.025 mol%, luminescence decay followed a single-exponential behavior and lifetimes of 1.94–2.21 ms were obtained for the four transitions of $^5D_4 \rightarrow {}^7F_{6,\ 5,\ 4,\ 3}$. Decay curves of the $^5D_3 \rightarrow {}^7F_{5,\ 4,\ 3}$ emission bands could not be measured due to their relatively low intensity.

Also for Tb^{3+}-doped ZABS, crystallization results in changes of the luminescence properties (Fig. 7). Generally, all crystallized samples exhibit significantly higher emission intensity, whereby maximum intensity of all emission peaks is found for the sample heat-treated at 800 °C/3 h. With crystallization, peak positions remain similar to those of the corresponding precursor glasses. For 377 nm as well as 350 nm excitation, all emission peaks appear increasingly Stark-split. Peaks originating from $^5D_3$ become significantly sharper (Fig. 7A). This indicates partitioning of Tb^{3+} into the crystalline phase, which reduces quenching of the upper lying $^5D_3$ level. Compared with the precursor glass, lifetime of all analyzed transitions is somewhat higher in the glass ceramic. For the intense green emission band, a value of 2.360 ms was found, but still appears to follow single exponential decay (noteworthy, the lifetime difference between glass and glass ceramic is too small to resolve distinct emission centers, if present). Time resolved emission spectra (Fig. 7B) reveal the absence of the three blue emission bands related to $^5D_3 \rightarrow {}^7F_{5,\ 4,\ 3}$ for a delay of ≥ 1 ms. As noted before, the high relative intensity of the $^5D_4$ radiative relaxation results from non-radiative decay of $^5D_3$ to $^5D_4$ and energy transfer between Tb^{3+} ions as follows [48]:

$$Tb^{3+}(^5D_3) + Tb^{3+}(^7F_6) \rightarrow Tb^{3+}(^5D_4) + Tb^{3+}(^7F_{2,1,0})$$

It is assumed that multi-phonon assisted non-radiative relaxation due to the low energy gap between $^5D_3$ and $^5D_4$ is the main mechanism for all the observed visible emission bands. As noted before, CR ($^5D_3 \rightarrow {}^5D_4 = {}^7F_6 \rightarrow {}^7F_0$) may be neglected due to relatively low dopant concentration.

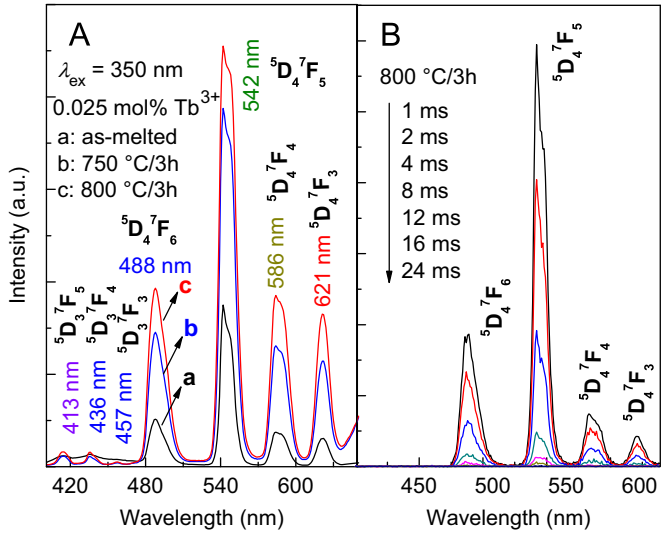

Fig. 7. Static (A) and dynamic (B) emission spectra of Tb^{3+} singly doped as-melted ZABS glass and corresponding glass ceramic.

3.3. Tb^{3+}/Mn^{2+} co-doped glasses

As a result of energy transfer from Tb^{3+} to Mn^{2+}, excitation of the dominant red emission peak of Mn^{2+} (645 nm) in Tb^{3+}/Mn^{2+} co-doped ZABS occurs over broad bands ranging from 330–380 nm and 400–450 nm (Fig. 8). In the spectral range of 330–380 nm, singly Tb^{3+}-doped ZABS exhibits only a weak excitation band. The excitation peak at 350 nm (Tb^{3+}: $^7F_6 \rightarrow {}^5L_9$) overlaps with the $^6A_1(S) \rightarrow {}^4E(D)$ transition of Mn^{2+}. Consequently, the intensity of the corresponding excitation band in Tb^{3+}/Mn^{2+}-co-doped ZABS is relatively higher than in either Mn^{2+} or Tb^{3+} singly doped glasses. Hence, the increase in photoemission from Mn^{2+} centers at 645 nm is related to energy absorption by Tb^{3+}. Additionally, emission from Tb^{3+} centers at 413 nm partially overlaps with the transition of $^6A_1(S) \rightarrow {}^4A_1(G)$, $^4E(G)$ in Mn^{2+} (414 nm), what leads to further increase in red photoemission from Mn^{2+}. If co-doped glasses are excited at 350 nm, the intensity of Tb^{3+}: $^5D_3 \rightarrow {}^7F_{5,4,3}/{}^5D_4 \rightarrow {}^7F_{6,5,4,3}$ emission peaks decreases significantly with increasing Mn^{2+}-concentration (Fig. 9A). At the same time, the intensity of the Mn^{2+}-related emission band from 575 to 700 nm ($^4T_1(G) \rightarrow {}^6A_1(S)$) increases (Fig. 9B). For various dopant concentrations, the relative emission intensity indicates that for 0.025 mol% Tb^{3+} co-doping, the maximum Mn^{2+} concentration should be around 1.0 mol% before self-quenching occurs.

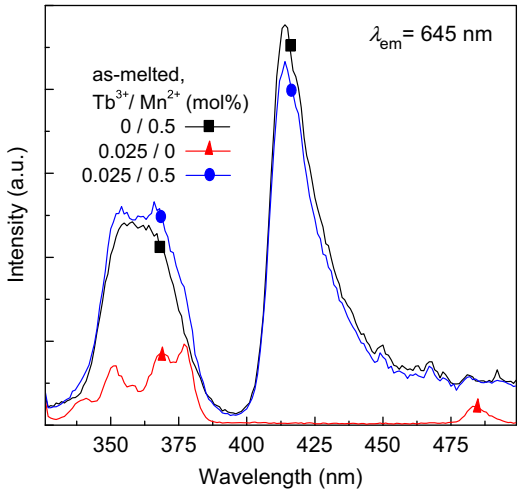

Fig. 8. Excitation spectra Mn^{2+}, Tb^{3+} singly and co-doped ZABS glass.

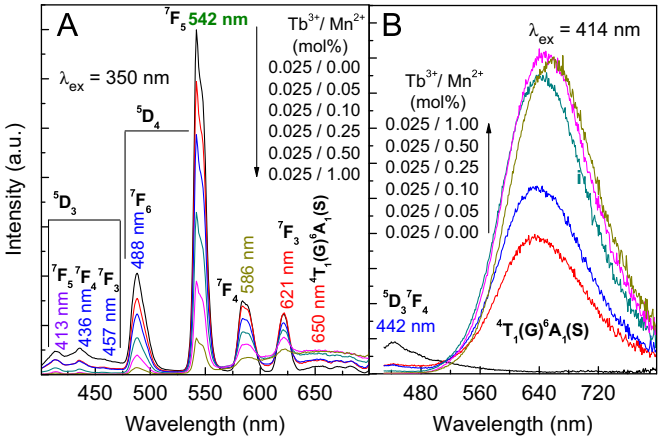

Fig. 9. Emission spectra of Tb^{3+}/Mn^{2+} co-doped glasses under 350 nm (A) and 414 nm (B) excitation for various Mn^{2+}-concentrations.

Dynamic luminescence analyses provide further evidence for the occurrence of energy transfer from Tb^{3+} to Mn^{2+}; considering decay of the green emission band at 542 of Tb^{3+} ($^5D_4 \rightarrow {}^7F_5$ transition) relative to Tb^{3+} singly doped ZABS reveals a significant decrease in emission lifetime, i.e., from 2.21 ms for the singly doped glass to 1.32 ms for 1.0 mol% Mn^{2+} co-doping. The decrease in lifetime is caused by fast non-radiative energy transfer from Tb^{3+} to Mn^{2+}.

3.4. Tb^{3+}/Mn^{2+} co-doped glass ceramics

Luminescence spectra of Tb^{3+}/Mn^{2+} co-doped ZABS glass ceramics reveal blue emission (413, 436, and 457 nm) due to Tb^{3+}: $^5D_3 \rightarrow {}^7F_{5,4,3}$ transitions, and green-red emission (488, 542, 586, and 621 nm) due to Tb^{3+}: $^5D_4 \rightarrow {}^7F_{6,5,4,3}$ including a broad red emission band (650 nm) associated with Mn^{2+} centers. For all Tb^{3+}-related emission bands, the intensity decreases gradually with increasing Mn^{2+}-concentration. At the same time, intensity of the Mn^{2+}-related emission band increases. Interestingly and in contrast to observations in singly doped glass ceramics, relative emission intensity is maximal for samples, which were annealed at 750 °C/3 h, and decreases somewhat for annealing at 800 °C/3 h (Fig. 10). Self-quenching appears to occur at a Mn^{2+}-concentration of 1.0 mol% for glass ceramics, which were produced at 750 °C, and 0.5 mol% for glass ceramics, which were produced at 800 °C. For heat treating at 800 °C/3 h, the Mn^{2+}: $^4T_1(G) \rightarrow {}^6A_1(S)$ band red-shifts to 660 nm and its intensity is strongly reduced. A similar observation is made for lower Mn^{2+}-content. As in Mn^{2+} singly doped ZABS, the red shift is associated with increasing exchange interactions between active ions. These observations indicate that Mn^{2+} and Tb^{3+} ions partition into the evolving nanocrystalline $ZnAl_2O_4$ phase to differing extent: The interionic distance between both species is the determining factor for the efficiency of the observed energy transfer process. It can be adjusted via a suitable heat treatment process. That is, the probability of energy transfer increases when crystal growth rate and number density are adjusted to enable minimum distance between Tb^{3+} to Mn^{2+}. This has immediate consequences on the color of photoemission and enables its tunability by the application of appropriate heat treatment procedures as well as combinations of dopant concentrations, i.e., from green to yellowish-red. Comparing the emission intensities of as-melted ZABS and corresponding glass ceramics, which were produced at different annealing temperatures, reveals maximal emission intensity for the glass ceramic prepared at 750 °C/3 h. Especially when excited at 414 nm, the intensity of red emission can be increased more than tenfold (Fig. 11). Based on

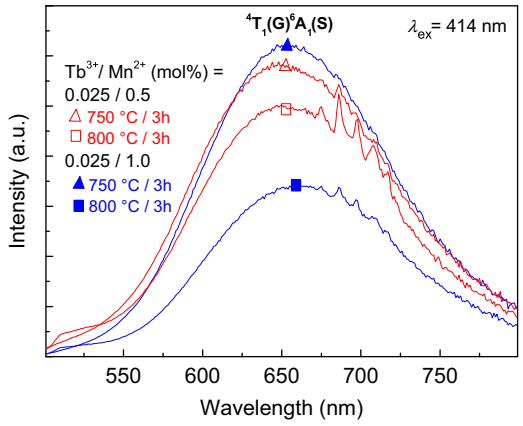

Fig. 10. Emission spectra of Tb^{3+}/Mn^{2+} co-doped ZABS glass ceramic after heat treatment for 3 h at 750 °C and 800 °C, respectively, for different Mn^{2+} concentrations, under 414 nm excitation.

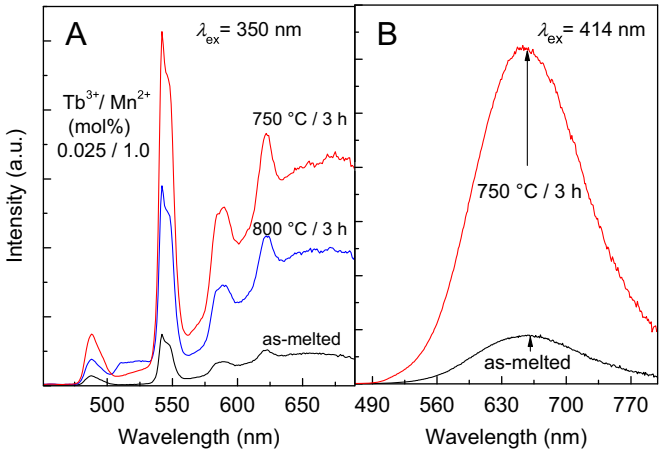

Fig. 11. Emission spectra of Tb^{3+}/Mn^{2+} co-doped as-melted ZABS glass and corresponding glass ceramic under 350 nm (A) and 414 nm (B) excitation.

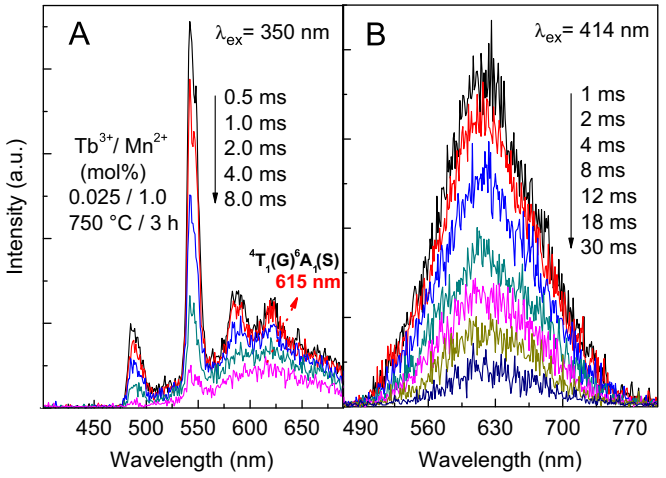

Fig. 12. Time resolved emission spectra of Tb^{3+}/Mn^{2+} co-doped glass ceramic under 350 nm (A) and 414 nm (B) excitation.

the observation of concentration quenching in Mn^{2+} singly doped ZABS, in the present study, we have limited the Mn^{2+} concentration to 1.0 mol%. We would expect that further enhancement of the red emission intensity may be possible by increasing the Mn^{2+}-concentration in co-doped ZABS glass ceramics to beyond 1.0 mol%. As with the co-doped as-melted glass, the lifetime of green emission from Tb^{3+} ions decreases with increasing Mn^{2+}-co-dopant concentration, i.e., from 2.36 to 1.88 ms. This is taken as further confirmation for the occurrence of energy transfer from Tb^{3+} to Mn^{2+} also in the glass ceramic, and further confirms that both Mn^{2+} and Tb^{3+} are incorporated into the crystal phase. Corresponding time-resolved emission spectra are shown in Fig. 12. For excitation at 350 nm, the emission bands related to Tb^{3+}: $^5D_4 \rightarrow {}^7F_{6,5,4,3}$ transitions are located at 488, 542, 586, and 621 nm. As with the Tb^{3+} singly doped material, the blue emission bands related to Tb^{3+}: $^5D_3 \rightarrow {}^7F_{5,4,3}$ cannot be observed due to fast non-radiative decay of $^5D_3$. As the delay time increases from 0.5 to 8 ms, the intensity of all Tb^{3+}-related emission bands decreases monotonically. A broad emission band appears at 615 nm (related to octahedral Mn^{2+} centers). This is a further reflection of energy transfer from Tb^{3+} to Mn^{2+} in the time interval of 8 ms. For 414 nm excitation, time resolved spectra are dominated by the broad emission band of Mn^{2+}: $^4T_1(G) \rightarrow {}^6A_1(S)$. Over a time of 30 ms, the intensity of this band decreases continuously. The position of the band remains unchanged,

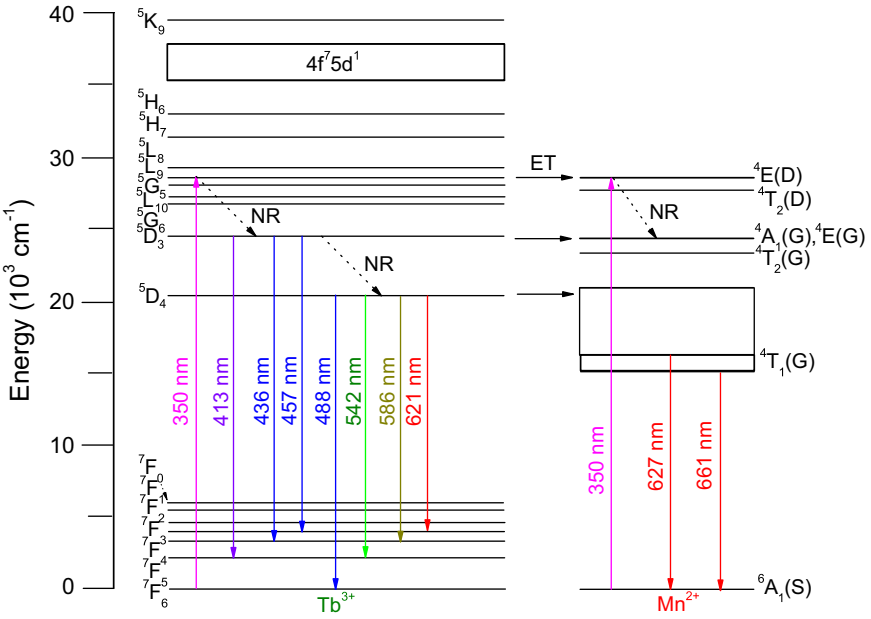

Fig. 13. Schematic of the energy transfer process from Tb^{3+} to Mn^{2+} ions.

indicating that emission occurs from a single active center. No Tb^{3+}-related emission bands can be observed at this excitation wavelength. For 350 nm excitation, the energy transfer process from Tb^{3+} to Mn^{2+} ions is described in the energy level scheme as shown in Fig. 13. It is observed that the respective $^5D_3$ and $^5D_4$ energy states of Tb^{3+} ions lie almost at the same level as $^4A_1(G)$, $^4E(G)$, and $^4T_1(G)$ energy levels of Mn^{2+} ions. When the Tb^{3+} ions are excited to the $^5L_9$ state (350 nm excitation), they non-radiatively relax to $^5D_3$, and further to $^5D_4$. The radiative transitions from $^5D_3$ and $^5D_4$ of Tb^{3+} to various $^7F_{j(j=3,\,4,\,5,\,6)}$ levels give rise to blue and green-red emission. On the other hand, a part of the energy from the $^5L_9$ state can be directly transferred to $^4E(D)$ of Mn^{2+}, which then relaxes non-radiatively to $^4A_1(G)$, $^4E(G)$; and further to $^4T_1(G)$, causing red emission. At 350 nm, Mn^{2+} ions are also directly excited to $^4E(D)$. In addition, Tb^{3+}: $^5D_3$ can partially transfer part of its energy directly to the $^4A_1(G)$, $^4E(G)$. Finally, energy transfer may also occur directly from $^5D_4$ of Tb^{3+} to $^4T_1(G)$ of Mn^{2+}. All these mechanisms lead to enhanced red emission from co-doped ZABS.

4. Conclusions

In summary, a series of Mn^{2+} or Tb^{3+} singly and codoped zinc–boroaluminosilicate glasses and corresponding gahnite glass ceramics were prepared and their structural and optical properties were studied. The controlled precipitation of nanocrystalline $ZnAl_2O_4$ from the glass matrix was confirmed by XRD analyses. Both Mn^{2+} and Tb^{3+} demonstrated partition into the crystallite phase, which is a prerequisite for efficient energy transfer between both species. Upon excitation at 350 and 414 nm, respectively, doped glasses and glass ceramics exhibit intense red photoemission (indicating octahedral coordination of Mn^{2+} emission centers). The position of the emission band red-shifts with increasing Mn^{2+} concentration. Energy transfer from Tb^{3+} to Mn^{2+} occurs dominantly upon 350 nm excitation and was confirmed by static as well as time resolved luminescence spectroscopy. In co-doped glasses and glass ceramics, the intensity ratio between green (Tb^{3+}) and orange or red (Mn^{2+}) emissions can be tuned by varying the concentration of Tb^{3+} (sensitizer) and Mn^{2+} (activator) ions, and also by varying the annealing procedure. In this way, the color of photoluminescence can be tuned.

Acknowledgments

Part of this work was supported by the Deutsche Forschungsgemeinschaft (DFG) through the Cluster of Excellence "Engineering of Advanced Materials—EAM". Funding from this source is gratefully acknowledged.

References

[1] H.J. Fan, A. Lotnyk, R. Scholz, Y. Yang, D.S. Kim, E. Pippel, S. Senz, D. Hesse, M. Zacharias, J. Phys. Chem. C 112 (2008) 6770–6774.
[2] V. Singh, R.P.S. Chakradhar, J.L. Rao, D.K. Kim, J. Lumin. 128 (2008) 394–402.
[3] V. Sreeja, T.S. Smitha, D. Nand, T.G. Ajithkumar, P.A. Joy, J. Phys. Chem. C 112 (2008) 14737–14744.
[4] B. Cheng, S. Qu, H. Zhou, Z. Wang, Nanotechnology 17 (2006) 2982–2987.
[5] X.Y. Chen, C. Ma, S.P. Bao, Z. Li, J. Colloid Interface Sci. 346 (2010) 8–11.
[6] C.D. Herná ndez-Pé rez, M. García-Hipó lito, M.A.Á. lvarez-Pé rez, O.Á. lvarez-Fregoso, F. Ramos-Brito, C. Falcony, Phys. Status Solidi A 207 (2010) 417–422.
[7] T. Suzuki, G.S. Murugan, Y. Ohishi, Appl. Phys. Lett. 86 (2005) 131903/1–3.
[8] S. Zhou, N. Jiang, H. Dong, H. Zeng, J. Hao, J. Qiu, Nanotechnology 19 (2008) 015702/1–6.
[9] D. Deng, S. Xu, H. Ju, S. Zhao, H. Wang, C. Li, Chem. Phys. Lett. 486 (2010) 126–129.
[10] R. Balda, S. García-Revilla, J. Fernández, V. Seznec, V. Nazabal, X.H. Zhang, J.L. Adam, M. Allix, G. Matzen, Opt. Mater. 31 (2009) 760–764.
[11] G. Gao, N. Da, S. Reibstein, L. Wondraczek, Opt. Express 18 (2010) A575–A583.
[12] G. Lakshminarayana, J. Qiu, M.G. Brik, I.V. Kityk, J. Phys. D: Appl. Phys. 41 (2008) 175106/1–10.
[13] G. Gao, S. Reibstein, M. Peng, L. Wondraczek, J. Mater. Chem. 21 (2011) 3156–3161.
[14] S. Yoo, U.-C. Paek, W.-T. Han, J. Non-Cryst. Solids 303 (2002) 291–295.
[15] T. Suzuki, K. Horibuchi, Y. Ohishi, J. Non-Cryst. Solids 351 (2005) 2304–2309.
[16] Y.V. Volk, I.A. Denisov, A.M. Malyarevich, K.V. Yumashev, O.S. Dymshits, A.V. Shashkin, A.A. Zhilin, U. Kang, K.-H. Lee, Appl. Opt. 43 (2004) 682–687.
[17] X.L. Duan, D.R. Yuan, Z..Liu, New Optical Materials and Nanophotonics, vol. 6796, Ottawa, Ontario, Canada, Proc. SPIE (2007) 67961S.
[18] Doris Ehrt, International Seminar on Science and Technology of Glass Materials (ISSTGM-2009), IOP Conference Series: Materials Science and Engineering 2 (2009) 012001/1–7.
[19] G. Gao, S. Reibstein, M. Peng, L. Wondraczek, Phys. Chem. Glasses: Eur. J. Glass Sci. Technol. B 52 (2011) 59–63.
[20] M. Kawano, H. Takebe, M. Kuwabara, Opt. Mater. 32 (2009) 277–280.
[21] T. Arai, Y. Arai, T. Takahashi, S. Adachi, J. Appl. Phys. 108 (2010) 063506/1–7.
[22] G. Lakshminarayana, J. Qiu, M.G. Brik, I.V. Kityk, J. Phys.: Condens. Matter 20 (2008) 335106/1–11.

[23] B. Wu, S. Zhou, J. Ruan, Y. Qiao, D. Chen, C. Zhu, J. Qiu, Opt. Express 16 (2008) 2508–2513.
[24] G. Lakshminarayana, H. Yang, J. Qiu, J. Solid State Chem. 182 (2009) 669–676.
[25] Y. Liu, Z. Zou, X. Liang, S. Wang, Z. Xing, G. Chen, J. Am. Ceram. Soc. 93 (2010) 1891–1893.
[26] R. Ye, S. Xu, D. Deng, Y. Hua, H. Wang, C. Li, S. Zhao, L. Huang, J. Lumin. 130 (2010) 2385–2389.
[27] C. Guo, X. Ding, L. Luan, Y. Xu, Sensors Actuators B 143 (2010) 712–715.
[28] G. Lakshminarayana, R. Yang, J.R. Qiu, M.G. Brik, G.A. Kumar, I.V. Kityk, J. Phys. D: Appl. Phys. 42 (2009) 015414/1–12.
[29] Q. Luo, X. Qiao, X. Fan, X. Zhang, J. Non-Cryst. Solids 356 (2010) 2875–2879.
[30] K. Liu, H.P. You, Y. Zheng, G. Jia, Y. Song, Y. Huang, M. Yang, J. Jia, N. Guo, H. Zhang, J. Mater. Chem. 20 (2010) 3272–3279.
[31] Y.H. Song, G. Jia, M. Yang, Y.J. Huang, H.P. You, H.J. Zhang, Appl. Phys. Lett. 94 (2009) 091902/1–3.
[32] C.F. Guo, L. Luan, F. Shi, X. Ding, J. Electrochem. Soc. 156 (2009) J125–J128.
[33] N. Da, M. Peng, S. Krolikowski, L. Wondraczek, Opt. Express 18 (2010) 2549–2557.
[34] Ch.L. Raju, N.O. Gopal, K.V. Narasimhulu, J.L. Rao, B.C.V. Reddy, Spectrochim. Acta—A 61 (2005) 2181–2187.
[35] A.S. Rao, B. Sreedhar, J.L. Rao, S.V.J. Lakshman, J. Non-Cryst. Solids 144 (1992) 169–174.
[36] H. Masai, T. Fujiwara, H. Mori, T. Komatsu, Appl. Phys. Lett. 90 (2007) 081907/1–3.
[37] X. Duan, D. Yuan, Z. Sun, C. Luan, D. Pan, D. Xu, M. Lv, J. Alloys Compd. 386 (2005) 311–314.
[38] G.S.R. Raju, H.C. Jung, J.Y. Park, C.M. Kanamadi, B.K. Moon, J.H. Jeong, S.-M. Son, J.H. Kim, J. Alloys Compd. 481 (2009) 730–734.
[39] A. Patra, G.A. Baker, S.N. Baker, J. Lumin. 111 (2005) 105–111.
[40] S. Kubota, T. Oyama, H. Yamane, M. Shimada, Chem. Mater. 15 (2003) 3403–3405.
[41] J.M. Nedelec, M. Bouazaoui, S. Turrell, Phys. Chem. Glasses 40 (1999) 264–268.
[42] X. Zhang, J. Zhang, L. Liang, Q. Su, Mater. Res. Bull. 40 (2005) 281–288.
[43] J.Y. Park, H.C. Jung, G.S.R. Raju, B.K. Moon, J.H. Jeong, J.H. Kim, J. Lumin. 130 (2010) 478–482.
[44] D. de Graaf, S.J. Stelwagen, H.T. Hintzen, G. de With, J. Non-Cryst. Solids 325 (2003) 29–33.
[45] D. Jia, J. Zhu, B. Wu, J. Lumin. 93 (2001) 107–114.
[46] A.J. Silversmith, D.M. Boye, K.S. Brewer, C.E. Gillespie, Y. Lu, D.L. Campbell, J. Lumin. 121 (2006) 14–20.
[47] T. Tsuboi, Eur. Phys. J. Appl. Phys. 26 (2004) 95–101.
[48] J.J. Velázquez, V.D. Rodríguez, A.C. Yanes, J. del-Castillo, J. Méndez-Ramos, J. Appl. Phys. 108 (2010) 113530/1–6.